Journal of Power Sources 188 (2009) 75–81

Contents lists available at ScienceDirect

Journal of Power Sources

journal homepage: www.elsevier.com/locate/jpowsour

Hydrogen electrocatalysts from microwave-synthesised nanoparticulate carbides

E.J. Rees, K. Essaki, C.D.A. Brady, G.T. Burstein*

Department of Materials Science and Metallurgy, University of Cambridge, Pembroke Street, Cambridge CB2 3QZ, UK

ARTICLE INFO

Article history:
Received 10 August 2008
Received in revised form
12 November 2008
Accepted 15 November 2008
Available online 28 November 2008

Keywords:
Microwave
Carburisation
Tungsten carbide
Fuel cell
Electrocatalyst

ABSTRACT

A comparison is presented of the electrocatalytic activity of tungsten carbide synthesised using microwave carburisation with that synthesised by furnace heating. Based on the resulting particle size, phase composition, passivity against corrosion and electrocatalytic activity for the hydrogen oxidation and evolution reactions, microwave synthesis appears to be a simple heating procedure which can be carried out more rapidly than conventional methods. Because microwave synthesis produces finer grain size than furnace heating, its products function better as electrocatalysts for both the hydrogen oxidation and evolution reactions. The role of KCl, Ni(II), Fe(II) and Mn(II) present as reactants during microwave synthesis is demonstrated. Also presented for the first time is the electrocatalytic activity obtained from tantalum carbide synthesised under microwave heating.

1. Introduction

Inexpensive electrocatalysts, synthesised from non-noble elements using a rapid, simple technique, would help the construction of fuel cells. As they promise much higher fuel efficiency than present power sources [1], and zero direct pollution, it is to be hoped that hydrogen–oxygen fuel batteries will soon prove sufficiently economical and practical to see widespread use. Tungsten carbide has been widely studied as a substitute electrocatalyst for hydrogen oxidation, as it has shown significant activity for this reaction as well as passivity in sulphuric acid electrolyte [2–4]. It also has a resistance to carbon monoxide poisoning [5], a problem that still mandates the use of uneconomic loadings of platinum-based catalysts when dealing with reformate hydrogen or air [6,7]. We have recently generated tungsten carbide using a solid state reaction in a furnace, and demonstrated a strong effect of trace KCl and Ni/Fe on the phases and grain size produced when carburising WO_3 with graphite [8]. However a method more rapid than furnace treatment is desirable. A promising method has been reported by Shen and co-workers, who have produced tungsten carbides by microwave heating, for use as a catalyst support [9–11]. Here, we develop a similar high temperature microwave synthesis and test the resulting carbides as electrocatalysts in their own right.

The effect of nickel and other transition metal additives on the catalytic activity of the carbides is of particular interest to us, given that we have previously seen significant electrocatalysis in a sputtered tantalum carbide system that was co-deposited with nickel [12]. Nickel–tungsten was also reported to be an alloy with improved electrocatalytic activity for the hydrogen evolution reaction [13]. We also demonstrate the versatility and thermal range of the microwave synthesis method by using the process to prepare tantalum carbide.

2. Experimental

Prior to microwave synthesis, mixtures of carbon and metal oxide were prepared as follows. Tungsten powder (1 g, 99.9%) was completely dissolved in 20 ml of 15% H_2O_2 in twice-distilled water, to give a pale yellow solution. For some precursors, admixants were added: either KCl alone (0.20 g, 99.9%), $MnCl_2$ (0.21 g), or KCl (0.20 g) together with nickel acetate (0.13 g) or $FeSO_4$ (0.15 g). Carbon powder (0.5 g, Vulcan XC-72R, Cabot) was then added. These quantities were scaled up in proportion when larger amounts of precursor were required, up to 9 g of precursor. The suspension was stirred for 48 h at room temperature, and then boiled dry. Tantalum does not dissolve in aqueous H_2O_2. The precursor for TaC was mixed by grinding together Ta_2O_5 (3.50 g, 99.99%, Aldrich, $< 5\,\mu m$) and XC-72R carbon powder (0.95 g) in a ceramic pestle and mortar for 30 min.

For furnace carburisation, as described previously [8], the precursor was placed in a ceramic boat and sealed in a 9 kW furnace which was then purged with argon (Air Products, BIP grade) at 5 $cm^3\,s^{-1}$ for 10 min with the outlet airlocked through a silicone oil bubbler. The system was heated under flowing argon to 1300 °C for 2 h at a temperature ramp rate of 300 °C h^{-1}.

* Corresponding author. Tel.: +44 1223 334 361
E-mail address: gtb1000@cam.ac.uk (G.T. Burstein).
URL: http://www.msm.cam.ac.uk/corrosion (G.T. Burstein).

0378-7753/$ – see front matter © 2009 Published by Elsevier B.V.
doi:10.1016/j.jpowsour.2008.11.074

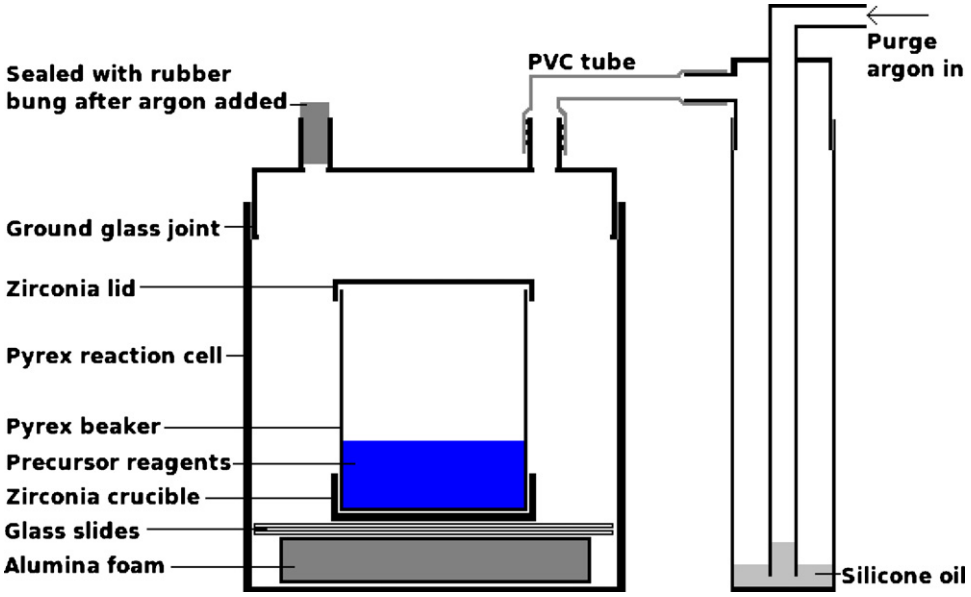

Fig. 1. Apparatus for microwave synthesis under argon.

For microwave heating we prepared a microwave-transparent reaction vessel, shown in Fig. 1. The precursor was placed in the inner Pyrex beaker, and the apparatus purged with argon at 3 cm^3 s^{-1}, with the outlet constricted to limit back-diffusion of air into the cell. After 10 min the outlet was sealed tightly, and the argon flow closed off 2 s later, so that the internal argon pressure was slightly above ambient. The silicone oil airlock then had the fluid in the inner tube pushed upward by 2–3 cm: this level did not subside during the minute prior to synthesis, confirming that the system was airtight. An airlock was needed to exclude oxygen from the reaction without risk from the pressure of hot gas evolved within the glassware. The vessel was placed in a commercial microwave oven (Belling, 900 W nominal, 2.45 GHz). Samples were heated typically at 50% microwave power for 4 min followed immediately by 80% for 4 min. The system was then allowed to cool for 60 min before collecting the product. The procedure was carried out in a fume cupboard because the production of CO was likely.

For scanning electron microscopy (SEM, in a JEOL 6340F microscope), the powders were mounted as thin-layer samples pressed into carbon tape that appears as a black background in the images below. X-ray diffraction (XRD) was used to assess phase composition and particle size. All powder diffraction traces were taken from 10° to 100° of 2θ, with a 0.05° step every 2.5 s, using CuK α radiation and a silicon monochromator.

Disc electrodes with particulate catalyst supported on carbon paper were fabricated as follows. 0.25 g of the synthesised powder, 1 ml of 5 wt% Nafion 117 solution (Aldrich), and 1 ml of twice-distilled water were mixed by ultrasonication for 5 min. The resulting paste was applied dropwise onto a 25 mm diameter disc of TGHP-090 carbon paper (Toray, supplied wetproofed with 20 wt% PTFE), with each applied layer dried until firm using a hairdryer. The assembled electrode was hydraulically pressed at 100 bar for 5 min at room temperature. If the catalyst layer detached at this step then the electrode was discarded; otherwise the flat, uniform electrode was tested for electrocatalytic performance and for passivity against corrosion.

Electrocatalytic activity was assessed by potentiostatic polarisation in a half cell made from polymethylmethacrylate (PMMA) modules, illustrated in Fig. 2. From right to left, the first module (right) holds the counter electrode, which was gold wire and foil. In electrochemical testing a gold counter electrode was chosen in preference to platinum, for stability and to obviate the possible transfer of highly catalytic contaminants onto the working electrode. The second module allows the electrolyte to be stirred and de-aerated by bubbling argon up a gas-lift arm. This gas-lift segment also allows the flowing electrolyte to be warmed by a nichrome heating coil, controlled by a home-built electronic feedback loop from the temperature sensor in the third module. As well as a thermistor, the third module contains a Luggin capillary for sampling and control of the working electrode potential. The capillary tip is 3 mm from the working electrode, and connects along a 30 cm polyvinylchloride tube to a side-arm that contains the reference electrode, which was held at room temperature. The fourth module (left) is a gas compartment, supplied at 3 cm^3 s^{-1} with either argon or hydrogen. Viton rubber seals were placed between each module before bolting the assembly together. The disc working electrode under test was sandwiched between the gas compartment and the reference module with a Viton rubber seal on both sides, and a gold foil annulus was placed against its edge on the gas side in order to provide an electrical connection to the potentiostat. The side of the disc coated with catalyst ink was faced into the electrolyte.

The cell was filled with 1.5 M sulphuric acid electrolyte, and operated at a temperature of 70 ± 0.5 °C. Prior to running potentiostatic tests, the oxygen content was minimised by bubbling pure argon through the cell for 45 min. The reference electrode was mercury–mercurous sulphate (MMS), in saturated K_2SO_4. Callibrated against a saturated calomel electrode, the MMS electrode potential was +0.414 V(SCE); thus the standard hydrogen equilibrium potential in these experiments was −0.655 V(MMS).

3. Results

During a typical microwave synthesis of WC, two types of visual behaviour were seen. After 2–3 min of heating, there was a flicker of orange-red flame from the reagents. From this time on, the reagents glowed with orange-yellow heat, which was brighter when the microwave-emitting magnetron was active. This appeared to be normal black body radiation. Intermittent white sparking was seen within the reagents, only when the magnetron was active, and the number of ember-like sparks declined as the synthesis progressed. Sparking is believed to be from metallic tungsten produced

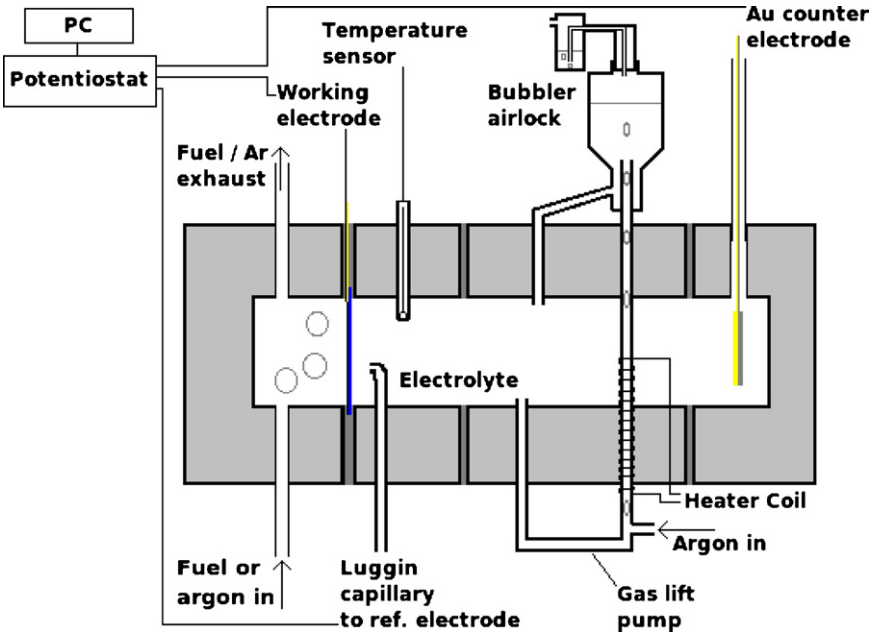

Fig. 2. Half cell for electrochemical testing.

by carbon reduction of its oxide but not yet carburised to WC. After the 8 min treatment ceased, the powder and crucible glowed with orange-red heat for 5–30 s longer. The inner Pyrex beaker was usually deformed by the heat, having flowed outward by 2–5 mm without breaking.

The XRD traces in Fig. 3 illustrate the progress of a microwave synthesis that started with 9 g of WO_3–C–KCl precursor. In the trace of the precursor WO_3 is visible, but the carbon and KCl were amorphous and never gave significant XRD signals. After 8 min of microwave heating, the graphitic carbon had reduced the tungsten oxide in the precursor to a variable mixture of W, WC and W_2C

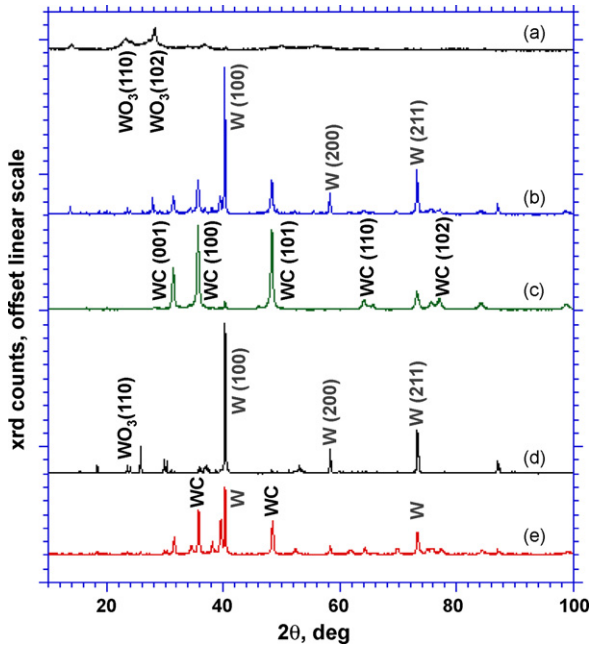

Fig. 3. XRD traces illustrating progression of carburisation during microwave treatment of a sample of WO_3–C–KCl: (a) precursor as-mixed, (b) after 8 min of microwave heating, and (c) after 16 min of heating. Also shown is the microwave carburisation of WO_3–C–$MnCl_2$; (d) the product after 16 min, and (e) 32 min.

phases. An additional 8 min gave near-complete carburisation to WC. For the manganese-doped precursor, WO_3–C–$MnCl_2$, the carburisation was slower and significant amounts of $MnWO_4$ remained unreacted after 16 min. This material required 32 min of microwave heating in order to give a yield of carbide that seemed comparable with the plain WO_3–C after 8 min. The phase compositions of the products of these syntheses are shown in Table 1, together with particle size estimates. The proportion of phases was assessed by the relative intensity of the XRD signal of each phase in the products, using X'Pert Pro software. Phase compositions found by this method are semi-quantitative. Scherrer grain sizes were assessed for the WC phase, and omitted where WC was too scarce to analyse. A range of peak widths were observed in each XRD signal, and the range given for Scherrer grain sizes corresponds to the uncertainty in peak broadening attributed to particle size.

Fig. 4 shows the XRD signals of the products formed after 8 min of microwave heating was applied to precursors with a variety of additives. The plain WO_3–C precursor retained about 34% of unreduced WO_3, along with a mixture of WC and W_2C. Addition of KCl led to all the oxide being reduced, producing an increased yield of WC, as well as some W_2C and metallic W. The WO_3–C–KCl–Ni precursor exhibited a higher yield of carbide: all intermediate W was carburised and WC was the main phase produced along with some W_2C. A tertiary phase was seen in the XRD trace of the nickel-admixed product that was identified as $Ni_{3.5}W_{9.4}C_{3.5}$. XRD did not reveal the presence of any KCl or chloride in the products.

Below are SEM images of the precursor for microwave synthesis, and of the products of microwave synthesis with and without admixants. The XC-72R carbon powder in the precursor forms rounded grains of about 50 nm diameter (Fig. 5). Microwaved WO_3–C forms a mixture of this precursor and faceted crystals of carbide that are 50–200 nm in size (Fig. 6). With KCl present the WC crystals remain 50–200 nm in diameter, but are clearly fused together and there is little unreacted precursor remaining (Fig. 7). Finally, nickel leads to striking grain coarsening of the tungsten carbide: the product shown in Fig. 8 has a grain size of 0.5–2 μm, and was identified as entirely carbide by XRD (Table 1).

Fig. 9 illustrates data taken during potentiostatic polarisation of a tungsten carbide particulate electrode (microwave synthe-

Table 1
Phase composition and particle size of carburisation products, listed by precursor and synthesis.

Precursor	Heating time	Phase composition (%)					Scherrer grain	SEM particle
		WC	W_2C	W	WO_3	Other	Size	Size
WO_3–C	Microwave 8 min	42	24	0	34		50–80 nm	50–100 nm
WO_3–C–KCl	Microwave 8 min	61	27	12	0		50–80 nm	50–200 nm
WO_3–C–KCl	Microwave 16 min	82	0	18	0		40–60 nm	50–100 nm
WO_3–C–KCl–Ni	Microwave 8 min	44	34	4	0	18% $Ni_{3.5}W_{9.4}C_{3.5}$	200–850 nm	300–2000 nm
WO_3–C–KCl–$FeSO_4$	Microwave 8 min	8	48	44	0		60–200 nm	
WO_3–C–$MnCl_2$	Microwave 16 min	3	0	50	15	32% $MnWO_4$		
WO_3–C–$MnCl_2$	Microwave 32 min	30	24	26	2	18% $MnWO_4$	40–100 nm	
WO_3–C	Furnace 8 h	55	42	3	0		80–140 nm	50–300 nm
WO_3–C–KCl	Furnace 8 h	81	0	19	0		80–140 nm	50–400 nm
WO_3–C–KCl–Ni	Furnace 8 h	99	0	1	0		150–800 nm	400–1500 nm
Ta_2O_5–C	Microwave 16 min					75%TaC, 25% Ta_2O_5	130–300 nm	60–400 nm

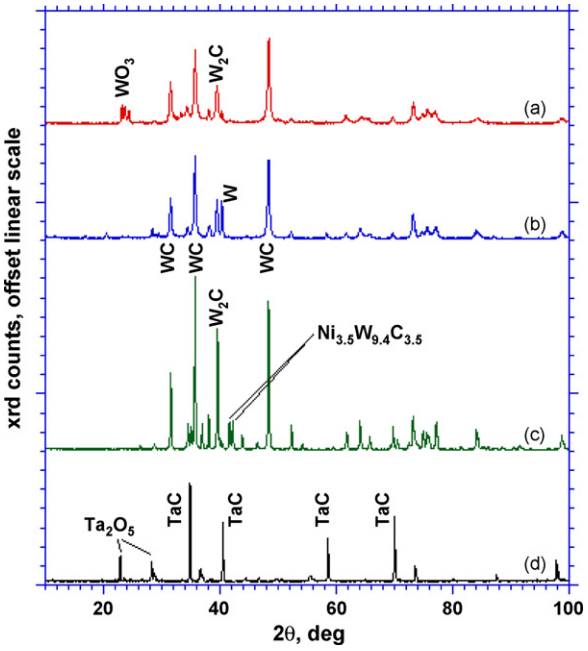

Fig. 4. XRD traces of the products from different compositions of precursor after 8 min of microwave heating: (a) from WO_3–C, (b) from WO_3–C–KCl, (c) from WO_3–C–KCl–Ni. Trace (d) is from Ta_2O_5–C after 16 min of heating.

sised from WO_3–C), showing current density against time. Positive currents are anodic. The magnitude of the nearly steady cathodic currents under argon after 100 s, and the size of the increase in steady anodic currents on changing argon for hydrogen, were interpretted, respectively, as hydrogen evolution and oxidation currents. For hydrogen oxidation, the gas fed to the electrode was switched from argon to hydrogen between 100 s and 250 s in the traces shown. There was a lag of about 50 s while the gas near the electrode was displaced and the current density switched from passivity to hydrogen oxidation, or back again. The increase in current density attributed to hydrogen oxidation was calculated by taking the anodic current at 200 s and subtracting the average of the values of the current at 100 s and 400 s. The background anodic current density measured after 400 s under argon was an indication of the passive corrosion rate of this electrode. This corrosion rate tended

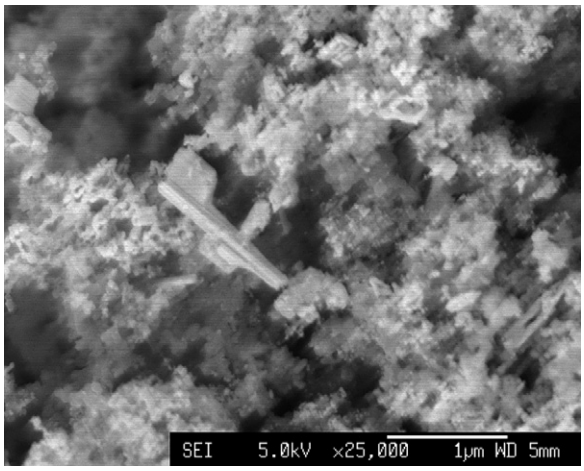

Fig. 6. SEM picture of WC from WO_3–C, microwaved for 8 min.

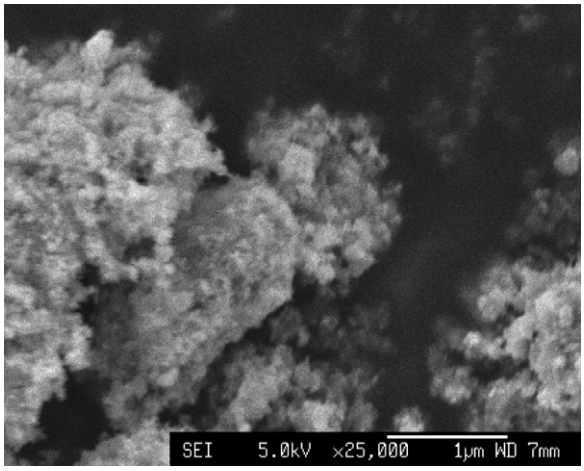

Fig. 5. SEM picture of precursor for microwave synthesis.

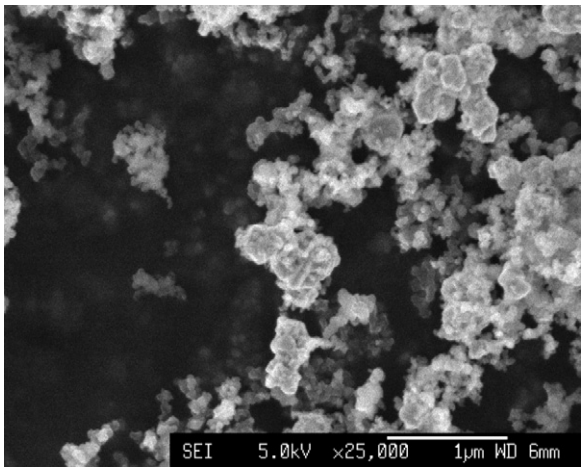

Fig. 7. SEM picture of tungsten carbide from WO_3–C–KCl, microwaved for 8 min.

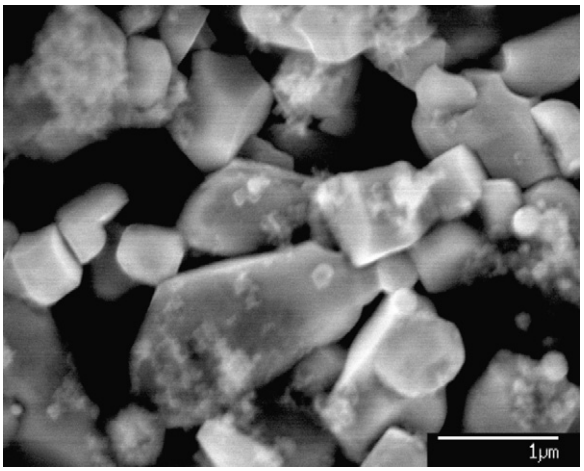

Fig. 8. SEM picture of tungsten carbide from WO_3–C–KCl–Ni, microwaved for 8 min.

towards 0.1 mA cm^{-2}, which represents significant passivity for a nanoparticulate material.

Tafel plots (Fig. 10) were generated from the results of potentiostatic experiments as described for Fig. 9, for various synthesised carbides. Fig. 10 a compares microwaved with furnace-heated tungsten carbides. The microwaved WO_3–C carbides transferred electrocatalytic hydrogen currents that were reproducibly twice as large as observed on the furnace-synthesised carbides, for both oxidation and evolution of H_2. For nickel-admixed tungsten carbides the microwaved products were more active for hydrogen evolution and similar for hydrogen oxidation, compared with the furnace-synthesised carbides. Both generated an order of magnitude less current than the plain tungsten carbides. Fig. 10 b records the electrocatalysis of hydrogen on carbides synthesised from precursors with various additives. Anodic oxidation of hydrogen, at a potential of −0.4 V (MMS) was observed to be 5–8 mA cm^{-2}on unadmixed WC, and on WC formed in the presence of KCl. The corresponding hydrogen oxidation rate was only 0.3 mA cm^{-2} on WC electrodes that were synthesised with admixed Ni, Mn, or Fe. The

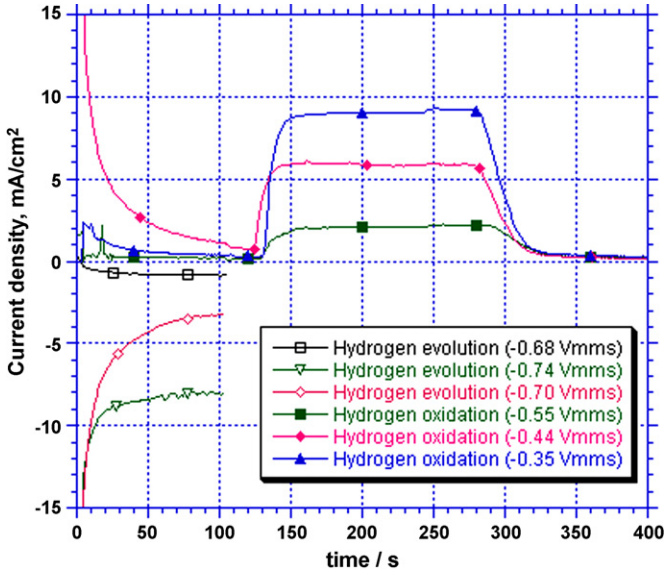

Fig. 9. Current density recorded during potentiostatic polarisation, at several different potentials, of a WC particulate electrode (WO_3–C precursor, microwaved for 8 min). Hydrogen evolution traces were taken under argon. Oxidation traces show the step up in anodic current on switching argon feed to hydrogen at 100 s, and then back at 250 s. Data points on these traces were recorded every second: the markers are for identification.

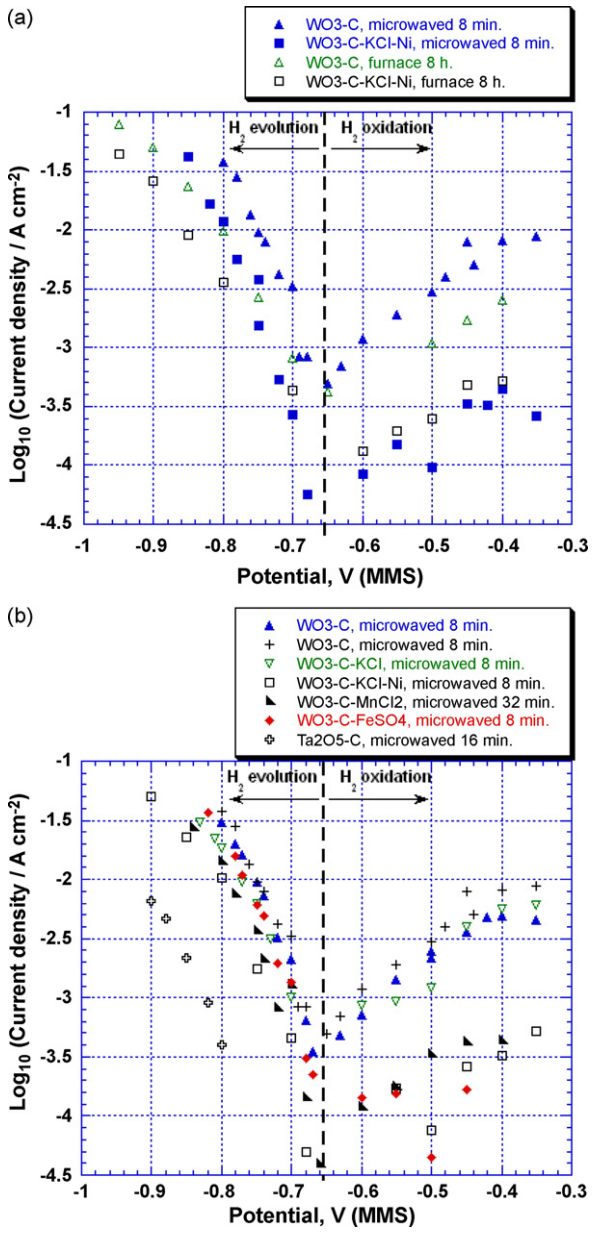

Fig. 10. Tafel plots showing the magnitude of electrocatalytic current density for hydrogen evolution (below −0.655 V(MMS), shown as a vertical line) and oxidation (above −0.655 V(MMS)), on particulate electrodes: (a) comparing microwaved with furnace-synthesised tungsten carbide, and (b) comparing microwave-synthesised carbides from precursors with various admixants.

Tafel slope ($\delta E/\delta \log i$) for hydrogen oxidation was 250 mV decade^{-1} on all the tungsten carbide electrodes. Cathodic evolution of hydrogen was more rapid than oxidation, because the observed Tafel slope was 95 mV decade^{-1} on all the tungsten (and tantalum) carbide electrodes. Furthermore, the disparity between the electrocatalytic current for plain tungsten carbide and nickel-admixed tungsten carbide is less for cathodic hydrogen evolution. At −0.8 V (MMS) the plain tungsten carbide catalysed hydrogen evoluion at 40 mA cm^{-2}, and the nickel-admixed carbide at 10 mA cm^{-2}. TaC produced negligible hydrogen oxidation, and lower hydrogen evolution current density than any WC particulate tested here: 0.4 mA cm^{-2} at −0.8 V(MMS).

4. Discussion

When microwaves of frequency f irradiate an electrically conductive material of resistivity ρ and relative permeability μ_r, we

Table 2
Metal oxide carburisation temperatures, from thermodynamic data [17].

Reaction	Minimum temperature
$WO_3 + 4C \rightarrow WC + 3CO$	620 °C
$2WO_3 + 5C \rightarrow 2WC + 3CO_2$	530 °C
$WO_3 + 3C \rightarrow W + 3CO$	700 °C
$2WO_3 + 3C \rightarrow 2W + 3CO_2$	690 °C
$Ta_2O_5 + 7C \rightarrow 2TaC + 5CO$	1040 °C
$2Ta_2O_5 + 9C \rightarrow 4TaC + 5CO_2$	1370 °C

expect their energy to be absorbed and dissipated as heat by eddy currents. The bulk of microwave energy (~ 85%) is absorbed within a skin depth, δ, given by Eq. (1) [14]. (μ_0 is $4\pi \times 10^{-7}$ N A^{-2}.)

$$\delta = \sqrt{\frac{\rho}{\pi f \mu_0 \mu_r}} \quad (1)$$

Under the 2.45 GHz microwaves, δ is calculated to be 32 μm in pure graphite, up to 3 mm in uncompressed XC-72R carbon powder, and 10 cm in the weakly conducting tungsten oxide (from resistivity data [15,16]). This suggests that, of the 20 mm diameter beaker of precursor material, only the outer volume was heated directly by induction and the core by subsequent thermal conduction inwards. The precursor particle size (< 100 nm) is smaller than δ, so the microwaves may penetrate deeper by scattering through free space between particles. If larger batches of material were to be processed, then the geometry of the precursor under microwave irradiation would have to be addressed so that the core is heated sufficiently. For this report, two consecutive 8 min treatments were sufficient to carburise fully 9 g of tungsten carbide precursor. In that case, the diameter of the reagents (20 mm) was still small enough that the centre of that material was carburised.

Calculations of the minimum temperatures required to make several carburisation reactions proceed were made using thermodynamic data [17], assuming unit activity for the gas products, with results presented in Table 2. The tantalum reaction reached 75% completion after 16 min of microwave heating (Fig. 3 and Table 1). Hence the microwave heating presumably generated temperatures above 1040 °C. This estimate is corroborated by the softening of the inner Pyrex beaker which indicates a temperature over about 830 °C [18], and by the crucible glowing with an orange heat indicating approximately 800–1100 ° C [19].

Microwave synthesis of tungsten carbide produced a mixture of phases (Table 1). Microwave products had phase compositions similar to those seen after furnace heat treatment, with the greatest similarity observed between products microwaved for 16 min and those furnace-heated for a total of 8 h. The microwave process can be faster and consume less energy because its apparatus has better thermal shock resistance and smaller thermal mass than a furnace. Heating the reagents for the minimum possible reaction time was more practical when using the microwave method. The particles of carbide produced by microwave heating had approximately half the Sherrer grain size of those furnace-heated (Table 1), an observation corroborated by the SEM particle size estimates. Microwaved particles were smaller most likely because they had less time at high temperature for the grains to grow. Fig. 10 a indicates that the finer microwaved carbides were more active electrocatalysts than furnace-heated carbides: the microwaved carbide electrodes generated approximately twice the current density for both hydrogen oxidation and evolution. The surface area of a given mass of particulate material scales inversely with the particle diameter. So the improved electrocatalysis of microwaved tungsten carbide may be fully explained by its increased specific surface area.

It appears that the carbide was produced progressively in the microwave synthesis, with WO_3 reduced first to W and subsequently carburised to WC (Fig. 3). Kodambaka made a similar report on the carburisation of tungsten oxide by graphite in a furnace [20]. There, the reagents proceeded from WO_3 to W, W_2C, and finally WC.

Additives had a strong influence on the synthesis of tungsten carbides (Fig. 4). KCl seemed to change the phase balance of the products by assisting the rapid reduction of WO_3. More metallic W was found in the products of KCl-admixed precursors, and the proportion of WC was also increased. KCl may assist the reduction of WO_3 to W by providing a molten flux that cleans the reacting surfaces. The improved yield of WC may arise from the more rapid initial reduction of WO_3 to W, which leaves more time for the carbide to be formed in the next step of the reaction.

Adding nickel as well as KCl increased the yield of tungsten carbide, to almost 100%. Also, the admixture of nickel into the precursor led repeatably to carbides with grain sizes an order of magnitude larger, seen both in SEM (Fig. 8) and indirectly by estimating the Scherrer grain size of WC within the synthesised products (Table 1). Conversion of tungsten to tungsten carbide and the growth of WC grains is facilitated by an intermediate phase of nickel tungsten carbide that reduces the activation energy for WC formation. Such an intermediate phase was observed in the XRD pattern of microwaved WO_3–C–KCl–Ni (Fig. 4). The phase was identified as $Ni_{3.5}W_{9.4}C_{3.5}$, and was previously seen as a trace impurity in a similar furnace-carburised product [8]. This effect on the grain size of microwave products is identical to the effect of nickel that we reported there for carburisation by furnace heating. The presence of nickel has previously been associated with increased grain growth of tungsten carbides synthesised by carburisation under hot ethane [21]. Addition of nickel to the WC precursor led to hydrogen oxidation current densities one order of magnitude lower, and currents about half an order of magnitude lower for hydrogen evolution. Metallic nickel is a good hydrogen electrocatalyst, and we have previously seen the addition of nickel has led to increased electrocatalysis, especially for sputtered materials [12,22]. But in these high-temperature syntheses, the principal effect of nickel was to limit the activity of electrodes composed of a certain mass of WC by promoting grain growth during its synthesis and so reducing the surface area for electrocatalysis.

Iron admixture also promoted grain growth of the carbide, but to a lesser extent than nickel. Iron seemed primarily to assist the formation of the W_2C phase, and still left about 40% of metallic tungsten (Table 1). Addition of iron led to electrocatalysts that were an order of magnitude less electrocatalytic for the hydrogen reaction than tungsten carbide from undoped WO_3–C (Fig. 10b). These electrocatalytic currents were similar to those seen on nickel-doped WC, but with iron the explanation is the production of less electrocatalytic phases as well as a degree of grain growth leading to reduced surface area. W_2C was a less effective hydrogen electrocatalyst than WC, as previously reported [23].

Admixing $MnCl_2$ into WO_3–C significantly impeded the formation of tungsten carbide phases. XRD (Table 1) indicated that $MnWO_4$ was formed, and this phase resisted reduction and carburisation. Prolonged microwave heating was needed to carburise the Mn-admixed precursor: 32 min compared with 8 min for an undoped precursor to yield 50% of carbide. The intensity-ratio analysis estimating the composition of the Mn-admixed product is approximate, since $MnWO_4$ shares strong XRD peaks with metallic W. WC and W_2C were produced in smaller proportions in the presence of manganese. Mn did not lead to significant grain growth of the WC particles. The low electrocatalytic activity of Mn-doped tungsten carbide is thus wholly due to the smaller amount of electrocatalytic WC phase. Although adding manganese led to a yield of WC phase that was only a third less than some additive-free tungsten carbides, the electrocatalytic currents were an order of magnitude lower (Fig. 10b). The electrocatalysis was disproportionately less than the yield of WC, probably because the fraction of WC was sufficiently low that there was not continuous contact between

the particles. The non-carbide phases present were likely to be electrically insulating, or metallic tungsten that would form a resistive oxide surface. So if the amount of WC was less than a percolation threshold then the resulting electrodes may be unable to collect current from the electrocatalytic phases that are present, leading to the substantial loss in performance seen with the Mn–WC electrode. It is important that synthesised electrocatalyst powders have a high enough proportion of WC that they avoid this problem. As discussed above, a KCl flux may be useful in obtaining this yield.

Electrodes made from separate batches of microwave-synthesised tungsten carbide showed that electrocatalytic current densities were reproducible to ±30%, (illustrated in Fig. 10 b for microwaved WO_3–C). Given that the range of currents seen during these experiments covered 3 decades, this reproducibility was good. TaC was two orders of magnitude worse than WC for the electrocatalysis of hydrogen evolution (Fig. 10b). This is expected, because TaC is not a strong hydrogen electrocatalyst, and indeed because the surface of TaC is likely to passivate by forming an electron-insulating oxide, Ta_2O_5. However TaC was found to be a useful material for electrocatalysis of oxygen reduction [12], so its microwave synthesis is noteworthy.

Throughout all tests of the gas diffusion electrodes, we observed a rate difference between hydrogen evolution and oxidation. Hydrogen evolution behaves as expected for a one-electron process: the observed Tafel slopes are always 95 ± 5 mV per decade increase in current. Hydrogen oxidation shows unfavorable response to overpotential: 200–300 mV per decade increase in current. The raised Tafel slope for hydrogen oxidation could be attributed to the difficulty of supplying hydrogen to the gas–liquid interface at the electrocatalyst surface. The flow of protons from the interface to the electrolyte apparently does not limit the reaction rate, since this would symmetrically suppress the current density for hydrogen evolution. However Fig. 10 records that hydrogen evolution was unimpeded by diffusion, up to at least 30 mA cm^{-2}. Whereas evolved hydrogen can easily escape a wet surface after it is produced, supplying H_2 through the liquid electrolyte at a diffusion-limited rate to the electrode surface may impede the hydrogen-oxidation process.

The hydrogen oxidation current density reaches a plateau, for all WC electrodes, as the electrode potential nears −0.4 V(MMS) (Fig. 10). This is apparently a diffusion limit to the supply of H_2 to these tungsten carbide particulate electrodes. The low limiting current for the hydrogen oxidation reaction results from the use of a too thick catalyst layer. The layer tends to fill with liquid electrolyte, through which the rate of diffusion of hydrogen gas is slow. Surprisingly, the diffusion-limited rate of hydrogen supply was not the same for all the electrodes. The electrodes made from more active electrocatalysts reached a diffusion limit of 8 mA cm^{-2} for hydrogen oxidation, whereas the less active electrodes seem to reach a lower plateau of 0.3 mA cm^{-2}. This is despite the electrodes being of identical thickness, which would suggest that the less active electrocatalysts would reach a plateau current density as high as the more active ones, albeit at a higher overpotential. So if the supply of hydrogen gas into the different carbide electrodes is limited by diffusive supply of gaseous H_2, then the trend may indicate faster gas transport through the layers with smaller particle size and smaller pores. Further reducing the particle size of WC should improve this.

5. Conclusions

(1) Microwave heating was used to produce WC and TaC, at temperatures in excess of about 1040 °C.
(2) Microwave synthesis was rapid: a 16 min microwave synthesis of WC produced similar results to an 8 h furnace treatment.
(3) The small thermal mass of the microwave apparatus allowed rapid heating and cooling, which was associated with smaller grains of product with higher mass-specific activity for hydrogen electrocatalysis than furnace-heated tungsten carbide.
(4) KCl provided a flux that promoted the reduction of WO_3, increasing the yield of the electrocatalytic WC phase.
(5) Manganese admixture to the tungsten carbide precursor led to the formation of $MnWO_4$ which slowed the carburisation reaction.
(6) Addition of nickel led to higher yields of the WC phase. An intermediate nickel-tungsten carbide phase assisted its formation.
(7) Transition metal salts promoted grain coarsening of tungsten carbide. The strength of this effect was Ni ≫ Fe > Mn ≈ KCl ≈ no additive.
(8) In microwave and furnace syntheses, nickel admixture led to WC particles approximately 10 times larger in diameter, with a concommitant order of magnitude decrease in the specific surface area and electrocatalytic current densities for cathodic hydrogen evolution and anodic hydrogen oxidation.

Acknowledgements

We gratefully acknowledge research studentships from the EPSRC, and a financial contribution from the New Zealand Foundation for Research, Science and Technology under contract no. C08X0409.

References

[1] J.O'M. Bockris, S. Srinivasan, Fuel Cells: Their Electrochemistry, McGraw-Hill, New York, 1969.
[2] C.J. Barnett, G.T. Burstein, A.R.J. Kucernak, K.R. Williams, Electrochim. Acta 42 (1997) 2381–2388.
[3] X.G. Yang, C.Y. Wang, Appl. Phys. Lett. 86 (2005) 224104.
[4] J.B. Christian, S.P.E. Smith, M. Stanley Whittingham, H.D. Abruna, Electrochem. Commun. 9 (2007) 2123–2128.
[5] D.R. McIntyre, G.T. Burstein, A. Vossen, J. Power Sources 107 (2002) 67–73.
[6] E. Christofferson, P. Liu, A. Ruban, H.L. Skriver, J.K. Norskov, J. Catal. 199 (2001) 123–131.
[7] H.A. Gasteiger, J.E. Panels, S.G. Yan, J. Power Sources 127 (2004) 162–171.
[8] E.J. Rees, C.D.A. Brady, G.T. Burstein, Mater. Lett. 62 (2008) 1–3.
[9] H. Meng, P.K. Shen, J. Phys. Chem. B 109 (2005) 22705–22709.
[10] M. Nie, P.K. Shen, M. Wu, Z. Wei, H. Meng, J. Power Sources 162 (2006) 173–176.
[11] M. Nie, P.K. Shen, Z. Wei, J. Power Sources 167 (2007) 69–73.
[12] D.R. McIntyre, A. Vossen, J.R. Wilde, G.T. Burstein, J. Power Sources 108 (2002) 1–7.
[13] E. Navarro-Flores, Z. Chong, S. Omanovic, J. Mol. Catal. A: Chem. 226 (2005) 179–197.
[14] D. Jiles, Introduction to Magnetism and Magnetic Materials, CRC Press, Boca Raton, 1998.
[15] D. Pantea, H. Darmstadt, S. Kaliaguine, L. Summchen, C. Roy, Carbon 39 (2001) 1147–1158.
[16] H. Kamal, A.A. Akl, K. Abdel-Hady, Physica B 349 (2004) 192–205.
[17] O. Kubaschewski, E.L.L. Evans, C.B. Alcock, Metallurgical Thermochemistry, 4th ed., Pergamon Press, Oxford, 1967.
[18] F. Moavenzadeh, R.W. Cahn, Concise Encyclopedia of Building and Construction Materials, MIT Press, 1990.
[19] J. Andrews, New Edge of the Anvil: A Resource Book for the Blacksmith, Rodale Press, Emmaus, PA, 1977.
[20] R. Koc, S.K. Kodambaka, J. Eur. Ceram. Soc. 20 (2000) 1859–1869.
[21] T. Xiao, H. Wang, A.P.E. York, V.C. Williams, M.L.H. Green, J. Catal. 209 (2002) 318–330.
[22] C.D.A. Brady, E.J. Rees, G.T. Burstein, Z.H. Barber, J. Electrochem. Soc. 155 (2008) B461–B466.
[23] C.D.A. Brady, E.J. Rees, G.T. Burstein, J. Power Sources 179 (2008) 17–26.